Linkages between the atmospheric transmission originating from the North Atlantic Oscillation and persistent winter haze over Beijing

Muyuan Li[12], Yao Yao[2], Ian Simmonds[3], Dehai Luo[2], Linhao Zhong[4], Lin Pei[5]

[1]Public Meteorological Service Center, China Meteorological Administration, Beijing, 100081, China

[2]Laboratory of Regional Climate-Environment for Temperate East Asia, Institute of Atmospheric Physics, Chinese Academy of Sciences, and University of Chinese Academy of Sciences, Beijing, China

[3]School of Geography, Earth and Atmospheric Sciences, University of Melbourne, Parkville, Victoria, 3010, Australia

[4]National Institute of Natural Hazards, Ministry of Emergency Management of China, 100085, Beijing, China

[5]Institute of Urban Meteorology, China Meteorological Administration, Beijing, 100089, China

Correspondence to: Yao Yao (yaoyao@tea.ac.cn)

Abstract. In this study, the persistent winter haze that occurred over Beijing during 1980 to 2016 is examined using reanalysis and station data. On both interannual and daily-to-weekly timescales, the winter haze weather in Beijing is found to be associated with a pronounced atmospheric teleconnection pattern from the North Atlantic to Eurasia (Beijing). A positive western-type North Atlantic Oscillation (WNAO+) phase and a positive East Atlantic/West Russia (EA/WR+) phase are observed as part of this teleconnection pattern (an arched wave train). This study focuses on the role of the WNAO pattern, because the WNAO+ pattern acts as the origin of the atmospheric transmission, 8–10 days before the persistent haze events. Further analyses reveal that the WNAO+ pattern can increase the number of haze days and persistent haze events on interannual and daily-to-weekly timescales. Specifically, strong WNAO+ winters (above the 95th percentile) can increase the number of haze days and persistent haze events by 26.0% and 42.3%, respectively. In addition, a high WNAO index for the five-day average (above the 95th percentile) predicts a 16.9% increase in the probability of haze days on Day 8 and a higher proportion of persistent haze days compared with an unknown WNAO state. Thus,

the WNAO+ pattern is as a necessary prior background condition for the formation of the wave train and is a skillful predictor for persistent hazy weather. Corresponding to the WNAO+ pattern, intensified zonal wind and a north–south sea surface temperature tripolar mode over the North Atlantic also appear before persistent haze events on the daily-to-weekly timescale. On the interannual timescale, winters with a greater number of persistent haze days are also associated with a tripolar SST mode over the North Atlantic that is situated farther northward.

1 Introduction

Beijing is the capital city of China and is situated in the northeast of the country. It covers 16,410 km^2 and has a permanent population of 21.542 million. In 2019, Beijing's gross domestic product reached 3,537 billion yuan, which was an increase of 6.1% over the previous year (http://www.stats.gov.cn). Along with economic development, Beijing has experienced more frequent hazy weather, especially persistent haze in winter, over the past 60 years (Wang et al., 2014; Su et al., 2015; Li et al., 2018a; Pei and Yan, 2018; Pei et al., 2018; Shi et al., 2019). Haze pollution is associated with a high concentration of particulate matter with a diameter of less than 2.5 micrometers ($PM_{2.5}$) and low visibility, which is harmful to human health (e.g., cardiovascular and respiratory diseases and lung cancer) and puts pressure on, among other things, public transportation and economic activities (Wang et al., 2013).

The serious impacts of haze pollution in Beijing have been the topic of numerous studies. High emissions of haze pollutants (e.g., black carbon and organic matter) contribute greatly to the formation of hazy weather in Beijing (Li and Han, 2016; Wu et al., 2016; Li et al., 2017). In addition, the atmospheric and meteorological conditions as well as external and remote influences, such as Arctic sea-ice concentration (SIC), snow cover across Siberia and sea surface temperatures (SSTs), also need

to be taken into consideration (An et al., 2019; Wang et al., 2020; Yin and Wang 2016, 2018). Atmospheric circulations that are favorable for hazy weather in Beijing include a weak East Asian winter monsoon (EAWM), a shallow East Asian trough and a northward shift of the East Asian jet (Chen and Wang, 2015; Zou et al., 2017; Pei et al., 2018; Wang et al., 2020). These circulations tend to reduce the intrusion of cold air to Beijing, and hence result in poor ventilation in winter (Zou et al., 2017; Pei et al., 2018). Furthermore, teleconnection patterns and wave trains also have potential impacts on haze over Beijing (Yin and Wang, 2017; Yin et al., 2017; Chen et al., 2019; Zhang et al., 2019; Chen et al., 2020a, b; Lu et al., 2020). Yin et al. (2017) analyzed the role of the positive phases of the East Atlantic/West Russia (EA/WR+) pattern, the western Pacific pattern and the Eurasia pattern in the increased number of hazy days over the North China Plain. They found that these climatic anomalies can lead to meteorological conditions that are conducive to the formation of haze pollution through modulating the anticyclonic anomalies over North China (Yin and Wang, 2017; Yin et al., 2017). The positive phase of the Arctic Oscillation (AO+) pattern can also increase the number of hazy days in Beijing (Lu et al. 2020). Years with a high AO index are accompanied by a weakened East Asian trough and a weakened Siberian high, which suppress the horizontal and vertical diffusion of haze pollutants (Lu et al. 2020). Chen et al. (2019) stressed the role of the positive phase of the North Atlantic Oscillation (NAO+), which is related to AO+, in inducing an anticyclone over northeast China, which favors haze pollution in North China in spring. Chen et al. (2020b) also studied autumn haze, and found that the relative importance of the external drivers seems to differ across the individual months of September, October and November. In addition, the winter haze weather in Beijing is directly affected by the local meteorological conditions. Many studies have suggested that static and relatively warm air, weakened northerly or even southerly winds, decreased relative humidity,

temperature inversion and downward air motion in the planetary boundary layer can suppress the dispersal and advection of haze pollutants (Wang et al., 2014; Zhang et al., 2014; Zhang et al., 2016; Wu et al., 2017; Wang et al. 2019; Zhong et al., 2019; Callahan and Mankin, 2020).

In addition, a reduction in Arctic Sea ice in autumn (as documented by Simmonds and Li 2021) can increase the number of subsequent winter haze days through weakening wave activity over eastern China (Wang and Zhang, 2015; Zou et al., 2017). Zou et al. (2017) also revealed that increased Eurasian snowfall in earlier winter leads to regional circulations unfavorable to the ventilation of pollutants. In addition, autumn Beaufort Sea ice is closely connected with the number of early-winter haze days in North China (Yin et al., 2019a; Li and Yin, 2020), while an increase in early-winter Chukchi Sea ice can intensify February haze pollution in North China (Yin et al., 2019b). The changes in sea ice in both the Beaufort Sea and the Chukchi Sea are linked to hazy weather in North China via modulated large-scale atmospheric circulations (e.g., the East Asian trough and teleconnections). SSTs in both the Atlantic and Pacific oceans have potential impacts on the occurrence of hazy weather (Xiao et al., 2015; Pei et al., 2018; Wang et al., 2019). Winter haze days in China are also associated with SST anomalies over the North Atlantic on decadal and interannual timescales via the Atlantic multidecadal oscillation, and are also related to SSTs over the South Atlantic on the interannual timescale by anomalous southerly airflow (Xiao et al., 2015). Pei et al. (2018) found that positive SST anomalies over the northwest Pacific are conducive to more winter haze days in Beijing through weakening of the EAWM system. Wang et al. (2019) also suggested that the interannual variability in autumn haze days in the Beijing–Tianjin–Hebei region is associated with a wave train induced by SSTs in the subtropical North Atlantic and a local meridional cell induced by SSTs in the western North Pacific.

Persistent haze events correspond to continuous pollution for several days, which not only has a broad impact on human life (through traffic jams, for example) but also threatens human health in many ways. In this study, we gain a better understanding of the physical processes and mechanisms of the persistent haze over Beijing. Local meteorological conditions are directly associated with hazy weather and usually show diurnal variations (Zhang et al., 2014; Li et al., 2018b; Li et al., 2019), while external influences, which vary slowly, play key roles in explaining the interannual and interdecadal variabilities in hazy weather (Wang et al., 2020). On intraseasonal timescales, large-scale atmospheric circulations (e.g., teleconnections and wave trains) can bridge the timescales of local meteorological conditions and external forces. Large-scale atmospheric circulations can be modulated by external forces and can influence local meteorological conditions. In previous studies, the atmospheric patterns associated with hazy weather were mainly obtained from linear correlation or composite analysis based on interannual or longer timescales (Yin and Wang, 2017; Yin et al., 2017; Chen et al., 2019; Lu et al., 2020). However, the evolution of the atmospheric circulations and their roles in the formation of hazy weather (especially persistent haze events) from daily to intraseasonal timescales are not clear. Thus, a more in-depth analysis of daily-to-weekly changes is needed to determine a more robust relationship between haze and atmospheric circulation and to test whether certain circulation patterns can help to improve the predictability of haze days and persistent haze events.

In this study, we focus on persistent winter haze over Beijing and the corresponding large-scale atmospheric circulations from the perspective of interannual and daily-to-weekly timescales. In particular, we examine the role of a western-type NAO+ pattern in the increase of haze on the interannual timescale and the improvement of forecast skill for winter haze on the daily-to-weekly timescale. Furthermore, we investigate the SST and Arctic Sea ice conditions that have been proposed

as drivers of large-scale atmospheric circulations.

2 Data and methods

2.1 Data

The observed relative humidity and visibility at 20 stations across Beijing at four local times (02:00, 08:00, 14:00 and 20:00) each day from 1980 to 2016 during the winter (December, January and February (DJF)) were obtained from quality-controlled station observations at the National Meteorological Information Center of China. The daily means of these variables were then calculated. Reanalysis data were taken from the European Centre for Medium-Range Weather Forecasts (ECMWF) ERA-Interim on a 1° × 1° grid (Dee et al., 2011). The variables included daily 500 hPa geopotential height (Z500), horizontal winds at 300 and 500 hPa, SST, SIC and sea-level pressure (SLP). We also used monthly SST and SIC data from the Hadley Centre Global Sea Ice and Sea Surface Temperature (HadISST) dataset (Rayner et al., 2003).

We used the normalized NAO index and EA/WR index from the National Oceanic and Atmospheric Administration/Climate Prediction Center (NOAA/CPC). Our investigation also employs a second NAO index, which is a modification of the NAO index proposed by Li and Wang (2003). Their index was taken as the difference in the normalized SLP, zonally averaged from 80° W to 30° E, between 35° N and 65° N. They commented that this measure "provides a much more faithful and optimal representation of the spatial–temporal variability associated with the NAO". We have slightly modified the Li and Wang (2003) definition by conducting our sector averaging over 80° W–10° W, instead of the original 80° W–30° E, and the newly calculated index is called the western-type NAO (WNAO) index. This modification is made because the longitudinal range of Li and Wang (2003) includes both the North Atlantic and part of the European continent. Atmospheric circulations

137 associated with Beijing haze in our investigation involve both a blocking anticyclone over Europe and
138 an NAO+ pattern (Figure 1a). When the anticyclone over Europe and the NAO+ pattern occur
139 concurrently, the center of the north pole of the NAO+ pattern is shifted westward, which displays a
140 western-type NAO+ type pattern. Although the NAO pattern is coupled with the anticyclone over
141 Europe, the modified WNAO index could better reflect the strength of the north–south dipole over the
142 Atlantic, regardless of the impact of the anticyclone over Europe. This concept was first proposed by
143 Yao and Luo (2014), who divided the NAO into the eastern-type NAO (ENAO) and the western-type
144 NAO (WNAO). They proposed this definition for the purpose of revealing the different relationships
145 between these two types of NAO and the downstream blocking (e.g. the Euro–Atlantic blocking),
146 temperature and precipitation. Some detailed NAO studies (Yao and Luo 2014; Luo et al. 2014; Yao
147 et al. 2016) have also revealed the disadvantages of the conventional NAO indices in the identification
148 of the spatial structures of the NAO pattern, and have suggested that the zonal position and inclination
149 of the NAO dipole could change the occurrence of extreme weather events. Below, we will see that
150 the WNAO index has a closer relationship to the Beijing haze frequency and better represents the
151 background circulation of the persistent haze events.

152 **2.2 Definition of persistent haze events**

153 Haze is generally defined in terms of relative humidity and visibility (World Meteorological
154 Organization, China Meteorological Administration, UK Met Office). Some studies also define haze
155 in terms of thresholds of PM2.5 concentrations (Cai et al. 2017; Callahan and Mankin 2020). As the
156 PM2.5 data are not available for a long time period and thus cannot cover our study period, we use a
157 definition more applied to meteorological range. In the "Specifications for surface meteorological
158 observations" compiled by the China Meteorological Administration (2004), haze is defined as a

159 weather phenomenon with a large amount of extremely fine dust particles evenly floating in the air
160 that reduces the horizontal visibility to less than 10 km. As visibility can also be reduced by fog, a
161 relative humidity threshold is also applied to distinguish hazy weather from fog. Many previous studies
162 (Wu, 2006, 2008; Yang et al., 2016; Pei et al., 2018; He et al., 2018) have proposed that fog is
163 associated with a relative humidity greater than 90%. Therefore, we use a daily mean relative humidity
164 of less than 90% and a visibility of less than 10 km as the criteria to define winter haze days in this
165 study (Pei et al., 2018; Chang et al., 2020). Persistent haze events are defined as periods for which
166 haze occurs for at least five consecutive days. The day with the minimum visibility within a persistent
167 haze event is defined as Day 0, which is the most prominent haze day, and the days before (after) Day
168 0 signify the growth (decay) of the haze event.

169 ## 3 Large-scale atmospheric circulations

170 ### 3.1 Interannual timescale

171 To show the context of the relationship between Beijing winter haze weather and atmospheric
172 circulations, in Fig. 1a we show the time series of the number of winter haze days (blue line) and
173 detrended winter haze days (red line) from 1980 to 2016. The linear trend (+1.9 days per decade) of
174 the number of winter haze days in Beijing is not significantly different from zero ($P = 0.10$), which is
175 consistent with previous studies (Chen and Wang, 2015; Pei et al., 2018, 2020), and its interannual
176 variability is quite large. Many factors could affect the interannual variation in the number of winter
177 haze days, including changes in emissions, emission reduction measures and climate variables (e.g.,
178 meteorological conditions, atmospheric circulation and SSTs) (Dang and Liao, 2019; Wang et al., 2020;
179 Pei et al. 2020). Pei et al. (2020) pointed out that anthropogenic emissions showed an increasing trend
180 before 2012 and a decreasing trend thereafter, which can be attributed to a Clean Air Action Plan

181 introduced in 2013, and these trends with opposite sign could explain the absence of a significant trend
182 in the number of hazy days. Thus, we undertake our investigation with detrended data to explore the
183 influences that are associated with the interannual variation in the number of hazy days. In addition,
184 the long-term trends are removed for winter haze days and other variables in the following analyses.

185 We focus first on the role of atmospheric circulation in inducing hazy weather on the interannual
186 timescale. The detrended winter haze days are significantly correlated with circulation patterns in the
187 Z500 anomaly field (Fig. 1b). A wave train of wavenumber-3 structure dominates the mid–high
188 latitudes; three cyclones are situated over the Greenland region, the Ural region and the Sea of Okhotsk
189 with positive geopotential height anomalies in between. The NAO+ and EA/WR+ teleconnections
190 patterns have been suggested to be connected with winter haze days in Beijing (Yin and Wang, 2017;
191 Yin et al., 2017; Chen et al., 2019). Barnston and Livezey (1987) have shown that the NAO+ pattern
192 is made up of negative geopotential height anomalies in the high latitudes of the North Atlantic
193 (Greenland) and positive anomalies over the central North Atlantic, extending into the eastern United
194 States and western Europe. The EA/WR+ pattern is associated with positive geopotential height
195 anomalies over Europe and northern China, and negative anomalies located over the central North
196 Atlantic and the north of the Caspian Sea. Following Barnston and Livezey (1987), we can say that
197 Fig. 1b demonstrates a western-type NAO+ pattern over the North Atlantic, as this pattern is situated
198 farther west and co-occurs with a blocking anticyclone over Europe. In addition, a quadrupole mode
199 from the North Atlantic to northern China shares some similarities with an EA/WR+ pattern, but there
200 are some differences. On the one hand, two negative geopotential height anomalies are located over
201 the northern North Atlantic and the northern Ural region, which are farther north than the two cyclones
202 of the EA/WR+ pattern. On the other hand, the EA/WR+ pattern shows a zonal wave train structure;

and only when the cyclone (north center of the western-type NAO+ pattern) over the North Atlantic is excluded can a tripolar mode from Europe to northern China manifest a zonal wave train structure.

To further understand the relationships between winter haze days in Beijing and the teleconnection patterns of the NAO and EA/WR, we present the annual variations in winter haze days, the NAO index and EA/WR index from NOAA/CPC, and the WNAO index in Fig. 2. Their correlation coefficients are calculated over the time periods 1980–2016, 1980–1999 and 2000–2016. The correlations between winter haze days and the NOAA/CPC NAO index are 0.27, 0.16 and 0.33, respectively, and only the correlation for the entire 1980–2016 period is significant at the 90% confidence level (Fig. 2a). Correlation coefficients between winter haze days in Beijing and the WNAO index are considerably larger for the 1980–2016 and 2000–2016 periods, being 0.42 ($P < 0.01$) and 0.61 ($P < 0.01$), respectively, while the correlation coefficient (0.08) is much smaller (and not significant) for the period 1980–1999 (Fig. 2b). This indicates that the WNAO index more strongly reflects the relationship between the north–south dipole mode over the North Atlantic and winter haze days in Beijing. The correlation with the EA/WR index is slightly lower than that with the WNAO index for the entire period (0.36, $P < 0.05$), but considerably higher (0.57, $P < 0.01$) when only the first 20 years of the record are considered (Fig. 2c). Overall, we see that the EA/WR+ pattern has a closer relationship with hazy weather in Beijing before 2000, whereas the western NAO+ pattern is dominant after that date. It is also worth noting that the extreme numbers of winter haze days more closely correspond with the magnitude of the WNAO index (Fig. 2d–f). We can see that the extremely low numbers of hazy days in the winters of 1995, 2003 and 2010 occur simultaneously with low (normalized) WNAO values of −1.11, −1.11 and −1.61, respectively, whereas the winter of 2013 with an extremely high number of hazy days has a large WNAO value of 2.42 (Fig. 2e). However, such

correspondences are weaker for the NOAA NAO index (Fig. 2d) and could not be found in the case of the EA/WR index (Fig. 2f).

3.2 Daily-to-weekly timescale

To cast further light on the above results, we have identified all the persistent haze events during 1980–2016 and explored the daily progression of the circulation structures that led up to (up to 10 days before) and followed (out to 8 days) the 65 identified persistent haze episodes. To accomplish this, we formed composites (across the 65 episodes) of daily Z500 anomalies and the horizontal components of wave activity flux (Takaya and Nakamura, 2001) (Fig. 3). From Day −10 to Day −8, a WNAO+ pattern can be identified over the North Atlantic, and the wave activity flux propagates downstream from the northern pole of the WNAO+ pattern to a weak anticyclone over Europe. Compared with the NAO pattern in the study by Li and Wang (2003), the north–south dipole mode of the WNAO pattern here is situated farther to the west and is accompanied by an anticyclone over Europe. These structures further emphasize the value of using our modified NAO index in this study. From Day −6 to Day −4, the weak anticyclone over Europe strengthens and a cyclone develops over western Russia following the propagation of wave activity. Simultaneously, the WNAO+ pattern weakens and shows a northeast–southwest inclination. From Day −3 to Day −2, an EA/WR+ pattern starts to appear in the mid to high latitudes. At this time, a zonal wave train that propagates from a cyclone over the North Atlantic, through an anticyclone over Europe and a cyclone over the west of Lake Baikal, to East Asia leads to the formation of an anticyclone over northeastern China. On Day −1, an anticyclone forms over the Gulf Stream region, which continues to provide wave activity to the development of downstream circulation. This anticyclone sustains the wave train propagating to northeastern China. As a result, the anticyclone over northeastern China persists for a total of 7 days from Day −3 to Day

3 and then moves eastward to the North Pacific. The wave train structure dissipates from Day 4, and the anomalous atmospheric circulation around Beijing becomes weaker.

From the daily evolution of atmospheric circulation, we find that certain teleconnection patterns (WNAO+ and EA/WR+) and wave trains lead to persistent haze events in Beijing. In the whole process, the WNAO+ pattern seems to be the origin of the transmission and the EA/WR+ pattern acts as a subsidiary mode that transfers the wave activities from the WNAO+ pattern to the downstream anticyclone over northeastern China. This sequence is consistent with the variations of zonal winds, as they act as waveguides for the propagation of wave trains (Ambrizzi et al., 1995; Fang et al., 2001; Athanasiadis et al., 2010; Wang and Zhang 2015; Martinez-Asensio et al., 2016; Wirth et al., 2018; Rudeva and Simmonds 2021). Zonal wind anomalies at 300 hPa are composited between Day −10 and Day 5 for the 65 persistent haze events to explain the evolution of large-scale circulations and to ascertain whether potential predictors exist (Fig. 4a). Corresponding to the propagation of the WNAO+ and EA/WR+ patterns, significantly intensified or weakened anomalous zonal wind centers can be clearly identified from the North Atlantic to East Asia. The negative–positive–negative zonal wind tripolar mode over the North Atlantic reflects the WNAO+ pattern, whereas the arched structure of the anomalous zonal wind from Greenland, passing through high latitudes to northern China, manifests in the EA/WR+ pattern. To track the daily variations in anomalous zonal winds, significantly increased zonal wind anomalies over the central North Atlantic, the Scandinavian Peninsula and the north of China are used as three indicators (Fig. 4b). The amplitude of the anomalous zonal wind over the central North Atlantic peaks at Day −8, which corresponds to the dominance of the WNAO+ pattern from Day −8 to Day −10 in Fig. 3. Although the zonal wind in this region weakens after Day −8, it retains significantly high values until Day 4. Simultaneously with the significantly increased zonal

wind over the central North Atlantic, the difference in the zonal wind over the south of the Scandinavian Peninsula and the zonal wind over North China also show significant positive anomalies starting from Day −11 and Day −5, respectively. The difference in the zonal wind over the south of the Scandinavian Peninsula reaches its highest point on Day −2 when the EA/WR+ pattern can be clearly identified in Fig. 3, whereas the anomalous zonal wind over the north of China reaches a peak on Day −1. From the analyses above, we can see that the three indicators of anomalous zonal winds well reflect the sequential occurrence of teleconnection patterns related to persistent haze events.

The above analysis demonstrates that the formation of the persistent haze weather in Beijing is closely related to the WNAO+ and EA/WR+ patterns. Although both patterns are essential in the persistent haze formation, the WNAO+ pattern plays the role of the starting point in the atmospheric transmission and leads to the formation of the persistent haze over a longer time period. In the next section, we determine whether the WNAO+ pattern is a harbinger of more persistent haze on interannual timescales and explore the extent to which the WNAO+ pattern can improve the haze prediction on the daily-to-weekly timescale.

4 The WNAO pattern and persistent Beijing haze

4.1 Interannual timescale

We first compare some characteristics of winter haze that occur in WNAO+ winters and WNAO− winters. The WNAO+ winters and WNAO− winters are classified with four sets of criteria with a view to making our results robust. We do this by stratifying the winters into above the 50th, 75th, 90th and 95th percentiles (WNAO+ winters) and below the 50th, 25th, 10th and 5th percentiles) (WNAO− winters). Figure 5a shows that there are more haze days in WNAO+ winters than in WNAO− winters. For the 50th, 75th, 90th and 95th percentiles, the average number of haze days for WNAO+ winters

291 are 4.5%, 23.2%, 57.5% and 38.6% more than their counterparts for WNAO− winters, and 2.3%, 7.4%,
292 22.8% and 26.0% more than the average numbers of all winters (the baseline) (Fig. 5a). This suggests
293 that the WNAO+ winters, especially winters with large-magnitude positive WNAO indices, are
294 conducive to haze days. For the persistent haze days (that is, haze days within persistent haze events),
295 their numbers for the WNAO+ winters are also greater than for WNAO− winters, and the same is true
296 for the persistent haze events (Fig. 5b,c). The differences are especially large for the 90th/10th and
297 75th/25th percentiles. For these two sets of criteria, the numbers of persistent haze days in WNAO+
298 winters are 167.9% and 101.5% more than that in WNAO− winters (Fig. 5b), whereas the numbers of
299 haze events in WNAO+ winters are 80.0% and 80.0% more than that in WNAO− winters (Fig. 5c).
300 Compared with the average numbers of persistent haze days (events) for all the winters, the numbers
301 for WNAO+ winters are increased by 14.2%, 24.3%, 57.7% and 80.8% (7.9%, 13.9%, 28.1% and
302 42.3%) at the 50th, 75th, 90th and 95th percentiles, respectively. The duration of haze events can be
303 derived by dividing the number of persistent haze days by the number of haze events. As can be seen,
304 the WNAO+ winters also correspond to longer persistent haze events, with the first two longest average
305 durations, 8.3 and 8.6 days, in the winters with WNAO indices larger than the 90th and 95th percentiles,
306 which are 2.9 and 2.7 days longer than that of winters with WNAO indices less than the 10th and 5th
307 percentile, respectively (Fig. 5d). These findings indicate that the WNAO+ pattern is conducive to the
308 occurrence and the persistence of winter haze in Beijing, whereas the WNAO− pattern militates against
309 these. These findings indicate that if we predict a strong WNAO+ winter (over the 95th percentile),
310 we are able to prognose a 26.0% increase in haze days, a 42.3% increase in haze events and 1.8 day
311 increase in haze duration compared with the condition that we do not know the prior state of the
312 WNAO.

4.2 Daily-to-weekly timescale

To test whether the predictability of haze days and haze events can be improved via the WNAO, we first compare the probability of haze days under three categories of conditions: the state of WNAO is unknown (the baseline), the WNAO is positive and the WNAO is negative. The WNAO we use here is a five-day (a pentad) moving average calculated by dividing the consecutive five-day sum of the WNAO index by five. To determine the probabilities of haze at different lead times, we take the last day of a pentad as Day 0, take the first day after the pentad as Day 1 and so on. We present the baseline probability of haze and the change in probability relative to the baseline when the WNAO is above (below) the 95th, 90th, 75th and 50th percentiles (the 50th, 25th, 10th and 5th percentiles) from Day 0 to Day 10 in Fig. 6. The baseline probability of a haze day for the 37 winters ranges between 42% and 43% (Fig. 6a). Moreover, the probabilities of haze for all percentiles are increased (decreased) given the positive (negative) WNAO condition, and most are significant at the 0.01 level (Fig. 6b,c). Compared with the 50th and 75th percentiles, larger increases in probability are found for the 95th and 90th percentiles, the peaks of which are at Day 8, being 16.9% and 13.0%, respectively. This suggests that the predictability of Beijing haze can be improved by 16.9% (13.0%) at Day 8 if the earlier five-day average WNAO is known to be larger than the 95th (90th) percentile. Moreover, the day on which the maximum probability occurs corresponds well with the obvious WNAO pattern at Day -8 of the composite haze events (Fig. 3). Conversely, a small WNAO index implies fewer winter haze days, especially at Day 5 for the 5th and 10th percentiles, being 19.0% and 12.0%, respectively. Hence, the earlier WNAO condition is conducive to the improvement of the prediction of winter haze day in Beijing.

As an extension of Fig. 6, Fig. 7 shows the proportions of persistent haze days in the haze days

under different WNAO states. If the WNAO state is unknown, the percentage of persistent haze days in the haze days varies between 29% and 32% (Fig. 7a). However, if the WNAO index is larger than the 95th, 90th, 75th and 50th percentiles, the percentage of persistent haze days increases to 50.6%, 45.1%, 45.8% and 37.5% on Day 7, Day 7, Day 8 and Day 6, respectively (Fig. 7b). This suggests that the positive WNAO pattern not only favors more haze days but also predicts a greater number of persistent haze days and haze events. However, if the WNAO is negative, persistent haze days and haze events are less likely to occur (Fig. 7c).

5 External influence of SST and SIC

5.1 Interannual timescale

We now determine the SST pattern in the North Atlantic and the SIC pattern in the Greenland Sea and Barents–Kara Sea, which might be related to persistent Beijing haze on the interannual timescale. Below we use the number of persistent haze days to categorize winters with more haze days and fewer haze days. This measure reflects the number of persistent haze events as well as their duration. The composite distributions of SST anomalies and SIC anomalies of 11 winters (1988, 1996, 1998, 2005, 2007, 2008 and 2011–15) with more than 15 persistent haze days and 11 winters (1980, 1982–84, 1986, 1987, 1994, 1995, 1999, 2003 and 2010) with no more than 5 persistent haze days, and their differences are shown in Fig. 8. The SST anomalies associated with the most persistent haze days show a north–south tripolar mode in the North Atlantic, with positive anomalies in the Gulf Stream region and negative anomalies at the southwest of the Canary Islands and regions around Greenland, which is consistent with the WNAO+ pattern (Fig. 8a). Simmonds and Govekar (2014) noted that warm SSTs in the Gulf Stream region give rise to a teleconnection pattern with a node in the Barents Sea and another over Eurasia. Significant SST anomalies can also be seen in the northwestern Pacific, with

357 negative SST anomalies from Yellow Sea to the Sea of Japan and positive SST anomalies to the east
358 of the Philippines. For SST anomalies of winters with fewer persistent haze days, a north–south tripolar
359 mode in the North Atlantic opposite to that in Fig. 8a is found, although the anomalies are not
360 significant (Fig. 8b). In addition, significant positive SST anomalies are located in the Greenland Sea
361 and the Barents Sea (Fig. 8b). The structure of the SST anomalies in the northwest Pacific is similar to
362 that in Fig. 8a, but with much smaller magnitude. Figure 8c, which shows the difference between
363 thesetwo anomaly plots, further highlights the distribution of SST anomalies that are associated with
364 more persistent haze days: a prominent north–south tripolar mode over the North Atlantic and negative
365 SST anomalies over the Greenland Sea and Barents Sea.

366 SIC anomalies in the Greenland Sea and Barents–Kara Sea also show significant differences
367 between winters with the greatest number of persistent haze days and winters with the lowest number
368 of persistent haze days (Fig. 8d–f). The Greenland Sea and the southern part of the Barents Sea are
369 dominated by positive SIC anomalies and the Kara Sea shows negative SIC anomalies, although they
370 are not significant (Fig. 8d). The only positive SIC anomalies that differ significantly from zero are
371 found in the north of the Barents–Kara Sea and the southeast of Greenland (Fig. 8d). By contrast, for
372 the lowest number of hazy days, composite significant negative SIC anomalies are located in the
373 Greenland Sea and the south part of the Barents Sea (Fig. 8e). The difference between Fig. 8d and Fig.
374 8e also suggests that the decrease in sea ice in the Greenland Sea and the southern Barents Sea is not
375 conducive to a greater number of persistent haze days or haze events (Fig. 8f).

376 **5.2 Daily-to-weekly timescale**

377 From the analyses on the interannual timescale, we can see that SST anomalies in the North
378 Atlantic and SIC anomalies in the Greenland Sea and Barents–Kara Sea are associated with the

occurrence of persistent haze days or haze events. To examine the potential causalities, here we analyzed the composite SST anomalies and SIC anomalies averaged over the period of 10 days prior to the first day of the 65 haze events. Prior to the persistent haze events, SST anomalies exhibit a north–south tripolar mode in the North Atlantic (Fig. 9a). This pattern differs from that shown in Fig. 8a; the tripolar mode is located farther south and has significant positive anomalies around the Florida peninsula and even into the Caribbean Sea and significant negative SST anomalies off the northeast coast of the United States (Fig. 9a). Figure 9a also shows significant negative SST anomalies in the Greenland Sea and the Barents–Kara Sea. For the SIC composite anomalies for these 65 events, we observe significant increases in the Greenland Sea and the Barents–Kara Sea (Fig. 9b). These prior distributions of SST and SIC anomalies are conducive to setting up the atmospheric circulations and zonal winds that are favorable for the formation of persistent Beijing haze events. The SST tripolar mode in the North Atlantic is favorable for the formation of a WNAO+ pattern, and the strongly increased zonal wind in association with the WNAO+ pattern encourages downstream wave train propagation. In concert with this, the decreased SST and increased SIC in the Barents–Kara Sea region potentially enable a strengthening of the cyclone upstream of the anticyclone over northern China, which is an essential part of the downstream wave train. Furthermore, as in Fig. 8a, the significant negative SST anomalies in the northwestern Pacific are not compatible with the anticyclone directly controlling persistent haze events in Beijing.

In light of the above, it is noted that, even though regression and composite analyses (e.g., Fig. 1) might suggest a strong link between haze events and the WNAO+, it is important to remember that such analyses identify *necessary* but not *sufficient* conditions (Boschat et al., 2016). This leads us to the question of whether there are persistent haze events related to the WNAO− pattern and what the

differences are between these haze events and those related to the WNAO+ pattern. First, the daily evolutions of the NAO index for the 65 persistent haze events (black line), 43 WNAO+-related persistent haze events (red line) and 22 WNAO−-related persistent haze events (blue line) are shown in Fig. 10. The composite WNAO index for all haze events reaches its highest value on Day −8, so we select a WNAO+-related (WNAO−-related) persistent haze event if its averaged WNAO index during the period of Day −10 to Day −6 is above (below) zero. Figure 10a shows that the daily evolution of the composite WNAO index for WNAO+-related and WNAO−-related persistent haze events generally shows the opposite character. However, the peak value (0.90) of the WNAO index for WNAO+-related persistent haze events appears on Day −8, the absolute value of which is larger than that of the valley value (−0.68) of the WNAO index for WNAO−-related persistent haze events on Day −10. Corresponding SST and SIC anomalies of the WNAO+-related case and the WNAO−-related case are also compared in Fig. 10b–d. We use the difference in the SST anomalies between the two regions A (40° N–55° N, 70° W–20° W) and B (22° N–37° N, 85° W–35° W) marked in Fig. 9a to signify the SST tripolar pattern in the North Atlantic. Daily evolutions of the SST anomaly difference show significant increases starting from Day −11 and Day −9 for the WNAO+-related case and all persistent haze events, respectively, whereas the difference in SST anomalies for the WNAO−-related case shows only a weak fluctuation (Fig. 10b). As for the SIC anomaly in the Barents–Kara Sea, it has a significant maximum amplitude leading the Day 0 of WNAO+-related persistent haze events by 12 days (Fig. 10d), whereas the SIC anomaly in the Greenland Sea shows significant high values during the period from Day −15 to Day 15 of WNAO−-related persistent haze events and its peak appears on Day −3 (Fig. 10c). We can conclude that the SST difference in the North Atlantic and SIC anomalies in the Barents–Kara Sea show preceding signals for WNAO+-related persistent haze events, and the

WNAO−-related persistent haze events are associated mainly with increased SIC anomalies in the Greenland Sea.

6 Conclusions and discussions

In this study, we have focused on persistent winter haze in Beijing from the perspective of large-scale atmospheric circulation (e.g., teleconnections and wave trains). We first presented the atmospheric circulation correlated with winter haze in Beijing on the interannual timescale. It is found that the frequency of winter haze is related to a western-type NAO+ pattern and an EA/WR+ pattern on interannual timescales. Notably, the number of winter haze days is more relevant to the WNAO+ pattern after 1999, whereas it is more associated with the EA/WR+ pattern before 2000. Then, the daily evolution of the composite circulation patterns and wave activities for 65 persistent haze events is used to represent the relationship between winter haze weather in Beijing and atmospheric circulation on the daily-to-weekly timescale. A transmission of atmospheric circulation demonstrated a wave train propagating from North Atlantic to northeast China. The WNAO+ pattern is the initiator of this transmission from Day −10 to Day −8, followed by an EA/WR+ pattern from Day −3 to Day −2. We also highlighted the daily variations in zonal winds linked to atmospheric circulation. It was revealed that the zonal wind over the central North Atlantic, which is coupled with the WNAO+ pattern, reached its largest value on Day −9, and the zonal wind downstream over the Scandinavian Peninsula and the north of China showed significantly increased values after Day −5, indicating the propagation of the wave train.

As the WNAO+ pattern acted as the original driver of this atmospheric transmission, we were interested in whether it can improve the predictability of winter haze on both interannual and daily-to-weekly timescales. From a comparison of the number of haze days and haze events, and the average

duration of haze events for WNAO+ winters, WNAO− winters and all winters with four sets of criteria, we found that the haze days and haze events are more likely to occur in WNAO+ winters. The WNAO+ winters contribute to a 22.8% (26.0%) increase in winter haze days, a 28.1% (42.3%) increase in winter haze events, 1.6- (1.8-) days increase in average haze duration relative to the baselines for the 90th (95th) percentile. Moreover, when compared to the WNAO− winters, these values are much higher. Thus, we propose that if the WNAO state can be predicted for a winter, then a general predication of the probability of haze days and haze events as well as the duration of haze events can be obtained.

On the daily-to-weekly timescale, our results also suggest that the WNAO+ pattern significantly improves the predictability of haze days and haze events. For a set of lead times (from Day 1 to Day 10) and four sets of criteria, the probabilities of haze days lagging the WNAO+ condition are all increased compared with the baseline or the WNAO− condition. The largest increase occurs for the 95th and 90th percentiles, and the largest increase, 16.9% and 13.0%, can be predicted at Day 8. However, if the WNAO index is lower than the 5th (10th) percentile, a (19.0%) 12.0% decrease of haze days can be predicted at Day 5. This provides more information for decision-makers for a given day, that is, if the five-day average of WNAO index of the day is known, they can determine the probability of haze for a set of days behind this day.

Further analyses revealed that the SST anomalies in the North Atlantic and SIC anomalies in the Greenland Sea and Barents–Kara Sea are also related to winter haze weather in Beijing on both interannual and daily-to-weekly timescales. On the interannual timescale, winters with a greater number of persistent haze days correspond to a north–south tripolar mode over the North Atlantic. On the daily-to-weekly timescale, a more southerly SST tripolar mode is also prominent over the North Atlantic, and the Greenland Sea and Barents–Kara Sea also show significant SST and SIC anomalies

10 days prior to the persistent haze events. For a more in-depth understanding, the relationship between the preceding WNAO pattern, SST and SIC anomalies and the persistent haze events was highlighted by comparing the WNAO+-related haze events and the WNAO−-related events. We found that the WNAO+-related case corresponded to prior SST signals in the North Atlantic and increased SIC anomalies in the Barents–Kara Sea, whereas the WNAO−-related case had large SIC anomalies only in the Greenland Sea.

Previous studies have shown that the large-scale atmospheric circulations are closely associated with the winter haze in Beijing from decadal timescales down to intra-seasonal timescales (Yin and Wang 2017; Yin et al. 2017; Chen et al. 2019). These studies well captured certain modes of atmospheric circulations that are significant during the haze episodes, but did not reveal their lead–lag relationships on a daily timescale as well as the role of atmospheric circulations in the prediction of winter haze. By analyzing the day-by-day evolutions, our investigation has revealed that a WNAO+ pattern, part of an atmospheric transmission, shows potential prediction abilities for persistent haze events. One step further, we find that prior knowledge of the WNAO state can significantly improve the predictability of haze days, and implies an increase in the predictability of persistent haze. As the external forces have longer memories and can affect the state of the NAO by air–sea interaction (Okumura et al. 2001; Frankignoul and Kestenare, 2005; Peng et al. 2002, 2003; Nie et al. 2019), it is possible to further improve the predictability of winter haze by predicting the WNAO state through external forces on both interannual and daily-to-weekly timescales. In addition, it is also worthwhile to determine the reasons why the WNAO index (EA/WR index) has a stronger correlation with winter haze weather in Beijing after 1999 (before 2000) from the perspective of climate change.

Data availability. Daily atmospheric and land-surface data were downloaded from the ECMWF ERA-Interim data archive (http://www.ecmwf.int/en/research/climate-reanalysis/era-interim) (ERA-Interim, 2017). Monthly sea surface temperature data and sea-ice concentration data are available from the Met Office Hadley Centre datasets (https://www.metoffice.gov.uk/hadobs/hadisst/data/download.html) (Met Office, 2017). The ground observations were taken from the National Meteorological Information Center of China (http://data.cma.cn/) (CMA, 2017). The NAO and EA/WR indices are from the NOAA Climate Prediction Center (http://www.cpc.ncep.noaa.gov/data/teledoc/telecontents.shtml) (CPC, 2017). The modified WNAO index can be obtained from the authors.

Competing interests. The authors declare that they have no conflict of interest.

***Author contributions*.** YY designed the study. ML created the figures. ML and YY wrote the manuscript. IS, DL and LZ gave constructive comments. LP provided and analyzed the observational station data.

Acknowledgments. The authors acknowledge support from the National Natural Science Foundation of China (Grants 41975068 and 41790473) and the National Key Research and Development Program of China (Grant 2016YFA0601802). Simmonds was supported by Australian Research Council Grant DP16010997. We also thank the two reviewers for their thoughtful and thorough comments.

References:

Ambrizzi, T., Hoskins, B. J., and Hsu, H. H.: Rossby-wave propagation and teleconnection patterns in the austral winter, J. Atmos. Sci., 52, 3661–3672, doi:10.1175/1520-0469(1995)052<3661:rwpatp>2.0.co;2, 1995.

An, Z., Huang, R. J., Zhang, R., Tie, X., Li, G., Cao, J., Zhou, W., Shi, Z., Han, Y., Gu, Z., and Ji, Y.: Severe haze in northern China: A synergy of anthropogenic emissions and atmospheric processes, P. Natl. Acad. Sci. USA, 116, 8657–8666, doi:10.1073/pnas.1900125116, 2019.

Athanasiadis, P. J., Wallace, J. M., and Wettstein, J. J.: Patterns of wintertime jet stream variability and their relation to the storm tracks, J. Atmos. Sci., 67, 1361–1381, doi:10.1175/2009jas3270.1, 2010.

Barnston, A. G., and Livezey, R. E.: Classification, seasonality and persistence of low-frequency atmospheric circulation patterns, Mon. Weather Rev., 115, 1083–1126, doi:10.1175/1520-0493(1987)115<1083:csapol>2.0.co;2, 1987.

Boschat, G., Simmonds, I., Purich, A., Cowan, T., and Pezza, A. B.: On the use of composite analyses to form physical hypotheses: An example from heat wave - SST associations, Sci. Rep., 6, 9, doi:10.1038/srep29599, 2016.

Cai, W., Li, K., Liao, H., Wang, H., and Wu, L.: Weather conditions conducive to Beijing severe haze more frequent under climate change, Nat. Clim. Chang., 7, 257–262, doi:10.1038/nclimate3249, 2017.

Callahan, C., and Mankin, J. The influence of internal climate variability on projections of synoptically driven Beijing haze, Geophys. Res. Lett., 47, doi:10.1029/2020GL088548, 2020.

Chang, L., Wu, Z., and Xu, J.: A comparison of haze pollution variability in China using haze indices based on observations, Sci. Total Environ., 715, doi:10.1016/j.scitotenv.2020.136929, 2020.

533 Chen, H., and Wang, H.: Haze days in North China and the associated atmospheric circulations based
534 on daily visibility data from 1960 to 2012, J. Geophys. Res.-Atmos., 120, 5895–5909,
535 doi:10.1002/2015jd023225, 2015.
536 Chen, S., Guo, J., Song, L., Li, J., Liu, L., and Cohen, J. B.: Inter-annual variation of the spring haze
537 pollution over the North China Plain: Roles of atmospheric circulation and sea surface temperature,
538 Int. J. Climatol., 39, 783–798, doi:10.1002/joc.5842, 2019.
539 Chen, S., Guo, J., Song, L., Cohen, J. B., and Wang, Y.: Temporal disparity of the atmospheric systems
540 contributing to interannual variation of wintertime haze pollution in the North China Plain, Int. J.
541 Climatol., 40, 128–144, doi:10.1002/joc.6198, 2020a.
542 Chen, S., Guo, J., Song, L., Cohen, J. B. and Wang, Y.: Intra-seasonal differences in the atmospheric
543 systems contributing to interannual variations of autumn haze pollution in the North China Plain,
544 Theor. Appl. Climatol., 141, 389–403, doi:10.1007/s00704-020-03221-4, 2020b.
545 China Meteorological Administration. Specifications for surface meteorological observation. Beijing:
546 China Meteorological Press, 129–130, 2004.
547 Dang, R., and Liao, H.: Severe winter haze days in the Beijing-Tianjin-Hebei region from 1985 to
548 2017 and the roles of anthropogenic emissions and meteorology, Atmos. Chem. Phys., 19, 10801–
549 10816, doi:10.5194/acp-19-10801-2019, 2019.
550 Dee, D. P., et al.: The ERA-Interim reanalysis: configuration and performance of the data assimilation
551 system, Q. J. Roy. Meteor. Soc., 137, 553–597, doi:10.1002/qj.828, 2011.
552 Fang, Z. F., Wallace, J. M., and Thompson, D. W. J.: The relationship between the meridional profile
553 of zonal-mean geostrophic wind and station wave at 500 hPa, Adv. Atmos. Sci., 18, 692–700,
554 doi:10.1007/BF03403494, 2001.

555 Frankignoul, C., and Kestenare, E.: Observed Atlantic SST anomaly impact on the NAO: An update,
556 J. Climate, 18, 4089–4094, doi:10.1175/jcli3523.1, 2005.
557 He, J., Gong, S., Zhou, C., Lu, S., Wu, L., Chen, Y., Yu, Y., Zhao, S., Yu, L., and Yin, C.: Analyses of
558 winter circulation types and their impacts on haze pollution in Beijing, Atmos. Environ., 192, 94–
559 103, doi:10.1016/j.atmosenv.2018.08.060, 2018.
560 Li, J., and Han, Z.: A modeling study of severe winter haze events in Beijing and its neighboring
561 regions, Atmos. Res., 170, 87–97, doi:10.1016/j.atmosres.2015.11.009, 2016.
562 Li, J., Du, H., Wang, Z., Sun, Y., Yang, W., Li, J., Tang, X., and Fu, P.: Rapid formation of a severe
563 regional winter haze episode over a mega-city cluster on the North China Plain, Environ. Pollut.,
564 223, 605–615, doi:10.1016/j.envpol.2017.01.063, 2017.
565 Li, J., Sun, J., Zhou, M., Cheng, Z., Li, Q., Cao, X., and Zhang, J.: Observational analyses of dramatic
566 developments of a severe air pollution event in the Beijing area, Atmos. Chem. Phys., 18, 3919–
567 3935, doi:10.5194/acp-18-3919-2018, 2018a.
568 Li, K., Liao, H., Cai, W., and Yang, Y.: Attribution of anthropogenic influence on atmospheric patterns
569 conducive to recent most severe haze over Eastern China, Geophys. Res. Lett., 45, 2072–2081,
570 doi:10.1002/2017gl076570, 2018b.
571 Li, J. P., and Wang, J. X. L.: A new North Atlantic Oscillation index and its variability, Adv. Atmos.
572 Sci., 20, 661–676, doi:10.1007/BF02915394, 2003.
573 Li, X., Gao, Z., Li, Y., Gao, C. Y., Ren, J., and Zhang, X.: Meteorological conditions for severe foggy
574 haze episodes over north China in 2016-2017 winter, Atmos. Environ., 199, 284–298,
575 doi:10.1016/j.atmosenv.2018.11.042, 2019.
576 Li, Y., and Yin, Z.: Melting of Perennial Sea Ice in the Beaufort Sea Enhanced Its Impacts on Early-

577 Winter Haze Pollution in North China after the Mid-1990s, J. Climate, 33, 5061–5080,
578 doi:10.1175/jcli-d-19-0694.1, 2020.
579 Lu, S., He, J., Gong, S., and Zhang, L.: Influence of Arctic Oscillation abnormalities on spatio-
580 temporal haze distributions in China, Atmos. Environ., 223, doi:10.1016/j.atmosenv.2020.117282,
581 2020.
582 Luo, D., Xiao, Y., Yao, Y., Dai, A., Simmonds, I., and Franzke, C. L. E.: Impact of Ural blocking on
583 winter warm Arctic-cold Eurasian anomalies. Part I: Blocking-induced amplification, J. Climate, 29,
584 3925–3947, doi:10.1175/jcli-d-15-0611.1, 2016.
585 Luo D., Yao, Y., and Feldstein, S.: Regime transition of the North Atlantic Oscillation and the extreme
586 cold event over Europe in January-February 2012, Mon. Wea. Rev., 142, 4735–4757,
587 doi:10.1175/MWR-D-13-00234.1, 2014.
588 Martinez-Asensio, A., Tsimplis, M. N., Marcos, M., Feng, X., Gomis, D., Jorda, G., and Josey, S. A.:
589 Response of the North Atlantic wave climate to atmospheric modes of variability, Int. J. Climatol.,
590 36, 1210–1225, doi:10.1002/joc.4415, 2016.
591 Nie, Y., Ren, H.-L., Zhang, Y.: The role of extratropical air–sea interaction in the Autumn subseasonal
592 variability of the North Atlantic Oscillation, J. Clim., 32(22), 7697–7712, doi:10.1175/JCLI-D-19-
593 0060.1, 2019.
594 Okumura, Y., Xie, S.-P., Numaguti, A.,Tanimoto, Y.: Tropical Atlantic air-sea interaction and its
595 influence on the NAO, Geophys. Res. Lett., 28(8), 1507–1510, doi: 10.1029/2000GL012565, 2001.
596 Pei, L., and Yan, Z.: Diminishing clear winter skies in Beijing towards a possible future, Environ. Res.
597 Lett., 13 (12), 124029, doi:10.1088/1748-9326/aaf032, 2018.
598 Pei, L., Yan, Z., Sun, Z., Miao, S., and Yao, Y.: Increasing persistent haze in Beijing: potential impacts

599 of weakening East Asian winter monsoons associated with northwestern Pacific sea surface
600 temperature trends, Atmos. Chem. Phys., 18, 3173–3183, doi:10.5194/acp-18-3173-2018, 2018.
601 Pei, L., Yan, Z., Chen, D., and Miao, S.: Climate variability or anthropogenic emissions: which caused
602 Beijing Haze? Environ. Res. Lett., 15 (3), 034004, doi:10.1088/1748-9326/ab6f11, 2020.
603 Peng, S. L., Robinson, W. A., and Li, S. L.: North Atlantic SST forcing of the NAO and relationships
604 with intrinsic hemispheric variability, Geophys. Res. Lett., 29 (8), 1276, doi:10.1029/2001gl014043,
605 2002.
606 Peng, S. L., Robinson, W. A., and Li, S. L.: Mechanisms for the NAO responses to the North Atlantic
607 SST tripole, J. Climate, 16, 1987–2004, doi:10.1175/1520-0442(2003)016<1987:mftnrt>2.0.co;2,
608 2003.
609 Rayner, N. A., Parker, D. E., Horton, E. B., Folland, C. K., Alexander, L. V., Rowell, D. P., Kent, E.
610 C., and Kaplan, A.: Global analyses of sea surface temperature, sea ice, and night marine air
611 temperature since the late nineteenth century, J. Geophys. Res.-Atmos., 108 (D14), 4407,
612 doi:10.1029/2002jd002670, 2003.
613 Rudeva, I., and Simmonds, I.: Midlatitude winter extreme temperature events and connections with
614 anomalies in the Arctic and tropics, J. Clim., 34, 3733-3749, doi:10.1175/JCLI-D-20-0371.1, 2021.
615 Shi, P., Zhang, G., Kong, F., Chen, D., Azorin-Molina, C., and Guijarro, J. A.: Variability of winter
616 haze over the Beijing-Tianjin-Hebei region tied to wind speed in the lower troposphere and
617 particulate sources, Atmos. Res., 215, 1–11, doi:10.1016/j.atmosres.2018.08.013, 2019.
618 Simmonds, I., and Li, M.: Trends and variability in polar sea ice, global atmospheric circulations and
619 baroclinicity, Ann. NY Acad. Sci., doi:10.1111/nyas.14673, 2021.
620 Simmonds, I., and Govekar, P. D.: What are the physical links between Arctic sea ice loss and Eurasian

winter climate?, Environ. Res. Lett., 9 (10), 101003, doi:10.1088/1748-9326/9/10/101003, 2014.

Su, B., Zhan, M., Zhai, J., Wang, Y., and Fischer, T.: Spatio-temporal variation of haze days and atmospheric circulation pattern in China (1961-2013), Quat. Int., 380, 14–21, doi:10.1016/j.quaint.2014.11.044, 2015.

Takaya, K., and Nakamura, H.: A formulation of a phase-independent wave-activity flux for stationary and migratory quasigeostrophic eddies on a zonally varying basic flow, J. Atmos. Sci., 58, 608–627, doi:10.1175/1520-0469(2001)058<0608:afoapi>2.0.co;2, 2001.

Wang, H., Xu, J., Zhang, M., Yang, Y., Shen, X., Wang, Y., Chen, D., and Guo, J.: A study of the meteorological causes of a prolonged and severe haze episode in January 2013 over central-eastern China, Atmos. Environ., 98, 146–157, doi:10.1016/j.atmosenv.2014.08.053, 2014.

Wang, H., Li, J. H., Peng, Y., Zhang, M., Che, H. Z., and Zhang, X. Y.: The impacts of the meteorology features on PM2.5 levels during a severe haze episode in central-east China, Atmos. Environ., 197, 177–189, doi:10.1016/j.atmosenv.2018.10.001, 2019.

Wang, N., and Zhang, Y. C.: Connections between the Eurasian teleconnection and concurrent variation of upper-level jets over East Asia, Adv. Atmos. Sci., 32, 336–348, doi:10.1007/s00376-014-4088-1, 2015.

Wang, J., Zhu, Z., Qi, L., Zhao, Q., He, J., and Wang, J. X. L.: Two pathways of how remote SST anomalies drive the interannual variability of autumnal haze days in the Beijing-Tianjin-Hebei region, China, Atmos. Chem. Phys., 19, 1521–1535, doi:10.5194/acp-19-1521-2019, 2019.

Wang, J., Liu, Y., Ding, Y., Wu, P., Zhu, Z., Xu, Y., Li, Q., Zhang, Y., He, J., Wang, J. X. L., and Qi, L.: Impacts of climate anomalies on the interannual and interdecadal variability of autumn and winter haze in North China: A review, Int. J. Climatol., 10, 4309–4325, doi:10.1002/joc.6471, 2020,

643 2020
644 Wang, Y. S., Yao, L., Liu, Z. R., J., D. S., Wang, L. L., and Zhang, J. K.: Formation mechanism and
645 control strategies of haze in China (in Chinese), Bull. Chin. Acad. Sci., 28, 353–363, 2013.
646 Wirth, V., Riemer, M., Chang, E. K. M., and Martius, O.: Rossby Wave Packets on the Midlatitude
647 Waveguide-A Review, Mon. Weather Rev., 146, 1965–2001, doi:10.1175/mwr-d-16-0483.1, 2018.
648 Wu, D.: More Discussions on the differences between Haze and Fog in City, Quat. Int., 32, 9–15, 2006.
649 Wu D.: Discussion on the distinction between haze and fog and analysis and processing of data,
650 Environ. Chem., 27(3): 327–330, 2008.
651 Wu, P., Ding, Y., and Liu, Y.: Atmospheric circulation and dynamic mechanism for persistent haze
652 events in the Beijing-Tianjin-Hebei region, Adv. Atmos. Sci., 34, 429–440, doi:10.1007/s00376-
653 016-6158-z, 2017.
654 Wu, Y., Zhang, R., Tian, P., Tao, J., Hsu, S. C., Yan, P., Wang, Q., Cao, J., Zhang, X., and Xia, X.:
655 Effect of ambient humidity on the light absorption amplification of black carbon in Beijing during
656 January 2013, Atmos. Environ., 124, 217–223, doi:10.1016/j.atmosenv.2015.04.041, 2016.
657 Xiao, D., Li, Y., Fan, S., Zhang, R., Sun, J., and Wang, Y.: Plausible influence of Atlantic Ocean SST
658 anomalies on winter haze in China, Theor. Appl. Climatol., 122, 249–257, doi:10.1007/s00704-014-
659 1297-6, 2015.
660 Yang, Y., Liao, H., and Lou, S.: Increase in winter haze over eastern China in recent decades: Roles of
661 variations in meteorological parameters and anthropogenic emissions, J. Geophys. Res.-Atmos., 121,
662 13050–13065, doi:10.1002/2016jd025136, 2016.
663 Yao, Y., Luo, D., Dai, A. and Feldstein, S.: The positive North Atlantic Oscillation with downstream
664 blocking and Middle East snowstorms: Impacts of the North Atlantic jet, J. Climate., 29, 1853–1876,

665 doi:10.1175/JCLI-D-15-0350.1, 2016.
666 Yao Y., and Luo, D.: Relationship between zonal position of the North Atlantic Oscillation and Euro-
667 Atlantic blocking events and its possible effect on the weather over Europe. Sci. China. Earth. Sci.,
668 57, 2628–2636, doi:10.1007/s11430-014-4949-6, 2014.
669 Yin, Z., and Wang, H.: The relationship between the subtropical Western Pacific SST and haze over
670 North-Central North China Plain, Int. J. Climatol., 3479–3491, doi:10.1002/joc.4570, 2016.
671 Yin, Z., and Wang, H.: Role of atmospheric circulations in haze pollution in December 2016, Atmos.
672 Chem. Phys., 17, 11673–11681, doi:10.5194/acp-17-11673-2017, 2017.
673 Yin, Z., Wang, H., and Che, H.: Understanding severe winter haze events in the North China Plain in
674 2014: roles of climate anomalies, Atmos. Chem. Phys., 17, 1642–1652, doi:10.5194/acp-17-1641-
675 2017, 2017.
676 Yin, Z., and Wang, H.: The strengthening relationship between Eurasian snow cover and December
677 haze days in central North China after the mid-1990s, Atmos. Chem. Phys., 18, 4753–4763, doi:
678 10.5194/acp-18-4753-2018, 2018.
679 Yin, Z., Li, Y., and Wang, H.: Response of early winter haze in the North China Plain to autumn
680 Beaufort sea ice, Atmos. Chem. Phys., 19, 1439–1453, doi:10.5194/acp-19-1439-2019, 2019a.
681 Yin, Z., Wang, H., and Ma, X.: Possible Relationship between the Chukchi Sea Ice in the Early Winter
682 and the February Haze Pollution in the North China Plain, J. Climate, 32, 5179–5190,
683 doi:10.1175/jcli-d-18-0634.1, 2019b.
684 Zhang, R., Li, Q., and Zhang, R.: Meteorological conditions for the persistent severe fog and haze
685 event over eastern China in January 2013, Sci. China Earth Sci., 57, 26–35, doi:10.1007/s11430-
686 013-4774-3, 2014.

687 Zhang, Y., Fan, J., Chen, X., Ashkenazy, Y., and Havlin, S.: Significant Impact of Rossby Waves on
688 Air Pollution Detected by Network Analysis, Geophys. Res. Lett., 46, 12476–12485,
689 doi:10.1029/2019gl084649, 2019.
690 Zhang, Z., Zhang, X., Gong, D., Kim, S. J., Mao, R., and Zhao, X.: Possible influence of atmospheric
691 circulations on winter haze pollution in the Beijing-Tianjin-Hebei region, northern China, Atmos.
692 Chem. Phys., 16, 561–571, doi:10.5194/acp-16-561-2016, 2016.
693 Zhong, W., Yin, Z., and Wang, H.: The relationship between anticyclonic anomalies in northeastern
694 Asia and severe haze in the Beijing-Tianjin-Hebei region, Atmos. Chem. Phys., 19, 5941–5957,
695 doi:10.5194/acp-19-5941-2019, 2019.
696 Zou, Y., Wang, Y., Zhang, Y., and Koo, J.-H.: Arctic sea ice, Eurasia snow, and extreme winter haze in
697 China, Sci. Adv., 3 (3), e1602751, doi:10.1126/sciadv.1602751, 2017.
698
699
700
701
702
703
704
705

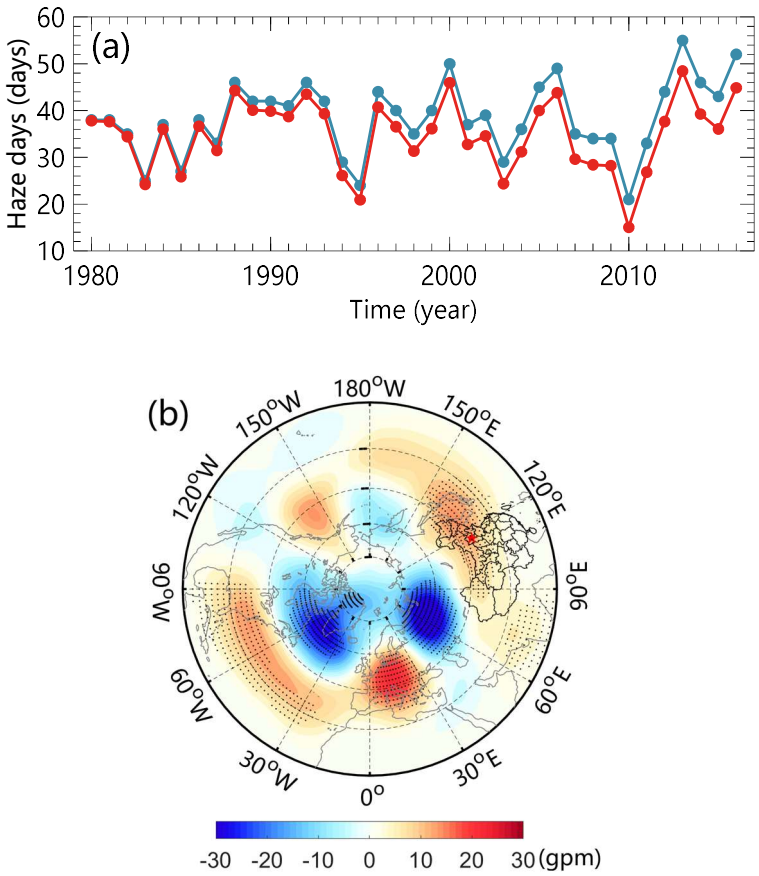

Figure 1. (a) Time series of winter haze days (blue) and detrended winter haze days (red) in Beijing from 1980 to 2016. To aid visualization, a fixed value is added to all the detrended data so that the first values of both series coincide. **(b)** Regressed Z500 anomalies (shading; units: gpm) against the detrended winter haze days. The dotted areas show values that are above the 95% confidence level based on a two-sided Student's *t*-test. For all plots in this study, the red star denotes the location of Beijing.

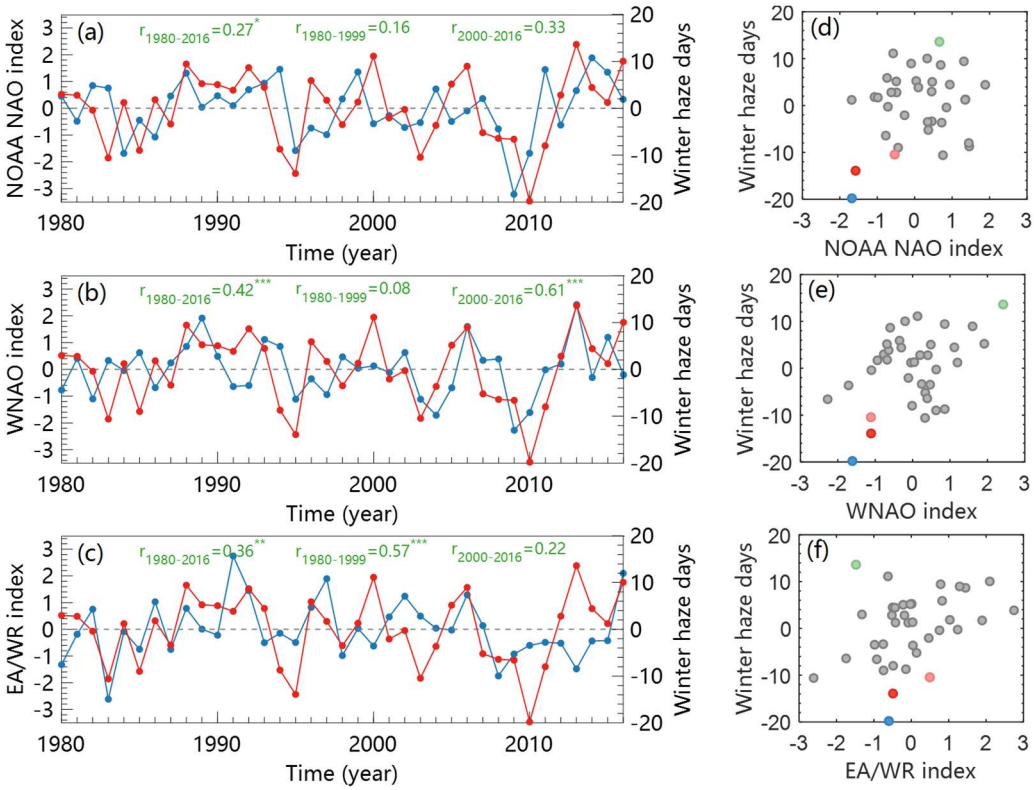

718

719 **Figure 2.** Time series of detrended winter haze days (red) and **(a)** NOAA NAO index (blue), **(b)**

720 WNAO index (blue) and **(c)** NOAA EA/WR index (blue). Correlation coefficients between winter

721 haze days and the three indices during the periods 1980–2016, 1980–1999 and 2000–2016 are labelled

722 at the top of each panel. The 90%, 95% and 99% confidence levels for the Student's *t*-test are denoted

723 by one, two and three asterisks, respectively. Scatter diagrams of winter haze days against the **(d)**

724 NOAA NAO index, **(e)** WNAO index and **(f)** EA/WR index, in which the red, pink blue and green

725 dots represent the year 1995, 2003, 2010 and 2013, respectively.

726

727

728

729

730

731

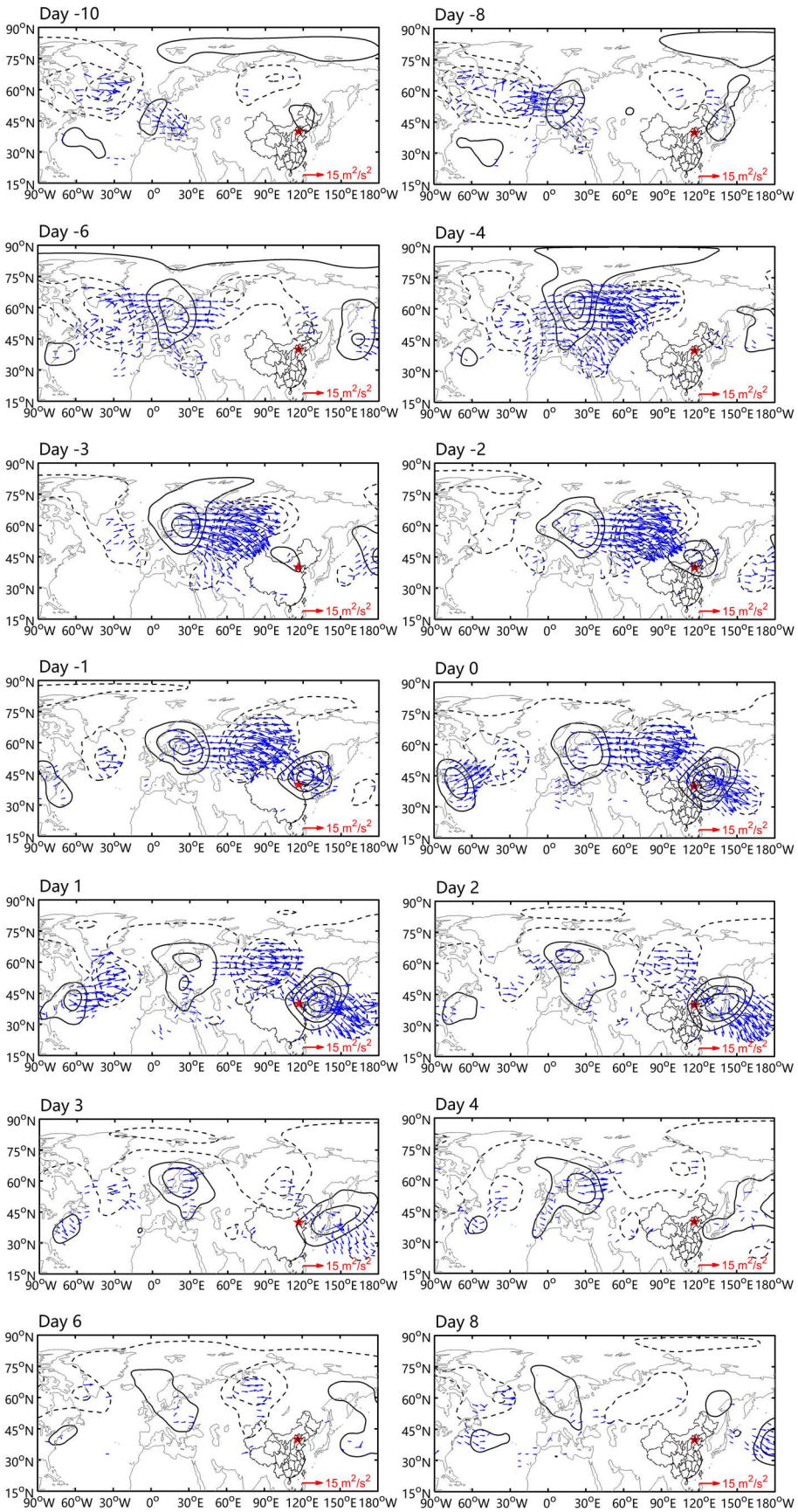

Figure 3. Instantaneous fields of the composite daily Z500 anomalies (contours, interval = 20; units:

gpm) and horizontal components of wave activity developed by Takaya and Nakamura (2001) (arrows; units: $m^2 s^{-2}$) from Day −10 to Day 8 for the 65 persistent haze events.

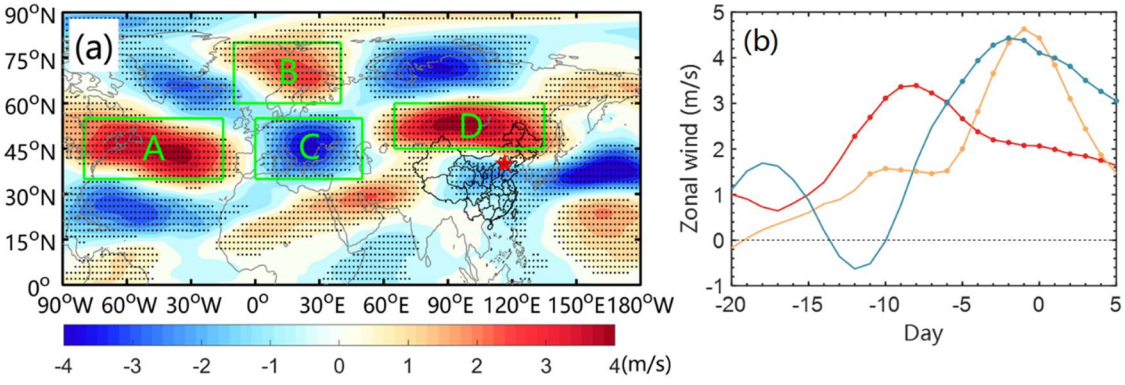

Figure 4. (a) Composite 300 hPa zonal wind anomalies (shading; units: m s^{-1}) between Day −10 and Day 5 for the 65 persistent haze events. The dotted areas show values that are above the 95% confidence level based on a two-sided Student's *t*-test. **(b)** Composite daily time series of region-averaged 300 hPa zonal wind anomalies in region A (80° W–15° W, 35° N–55° N) (red) and region D (65° E–135° E, 45° N–60° N) (orange) and the difference in region-averaged zonal wind anomalies between region B (10° W–40° E, 60° N–80° N) and region C (0° W–50° E, 35° N–55° N) (blue). The dots denote the days with values that are above the 95% confidence level for the two-sided Student's *t*-test.

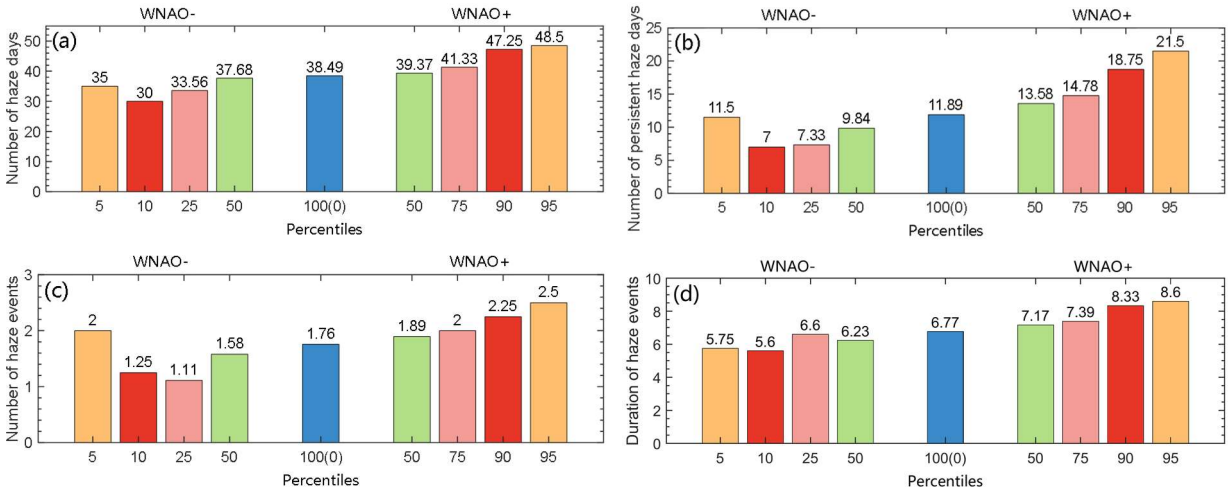

Figure 5. Average number of **(a)** haze days, **(b)** persistent haze days, **(c)** haze events and **(d)** average duration of haze events (days) during WNAO− winters and WNAO+ winters. The orange, red, pink and green bars on the left and right denote winters with a WNAO index larger than the 5th, 10th, 25th and 50th percentiles (WNAO− winters) and winters with the WNAO index smaller than the 95th, 90th, 75th and 50th percentiles (WNAO+ winters), respectively. The blue bars in the middle denote the results of all the winters. The persistent haze days are defined as haze days belonging to haze events.

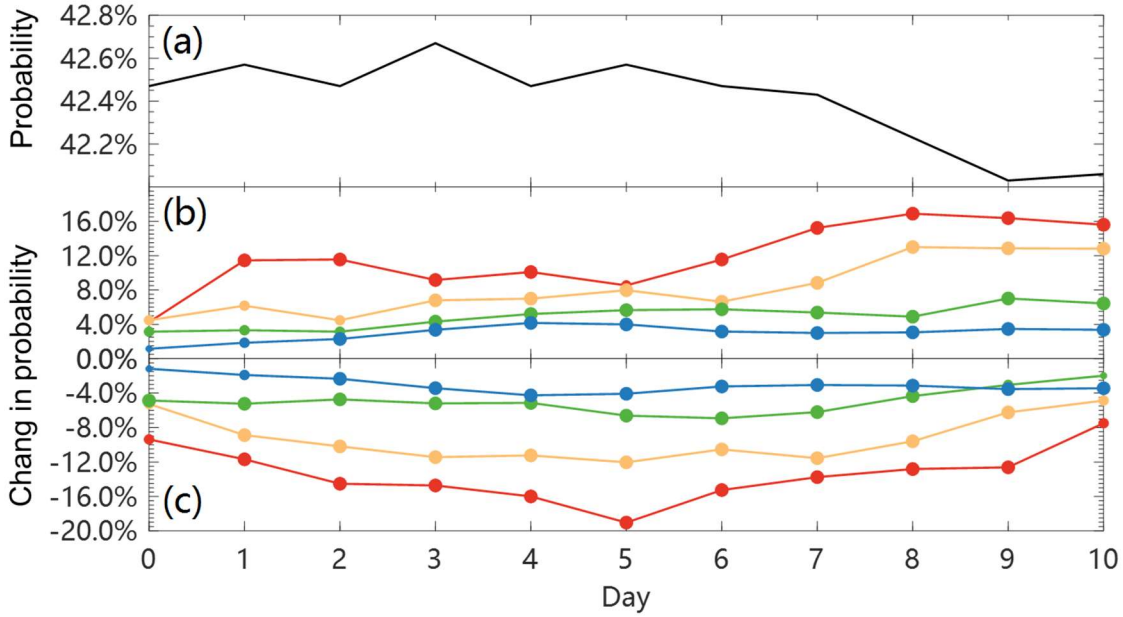

773

774 **Figure 6.** The probability of haze day at Day i ($i = 0 \ldots 10$) when **(a)** the state of the WNAO is unknown.
775 The change in probability of haze day compared with **(a)** on the condition that **(b)** the five-day moving
776 average WNAO index is above the 95th (red), 90th (yellow), 75th (green) and 50th (blue) percentile
777 of the moving average series, and **(c)** the five-day moving average WNAO index is below the 50th
778 (blue), 25th (green), 10th (yellow) and 5th (red) percentiles of the moving average series. The five-day
779 moving average is the five-day sum of the WNAO index divided by five. Day 0 is defined as the last
780 day of each consecutive five days. The small, medium and large dots represent the probability changes
781 that are above the 90%, 95% and 99% confidence levels, respectively, for a Monte Carlo test with
782 10,000 simulations.

783

784

785

786

787

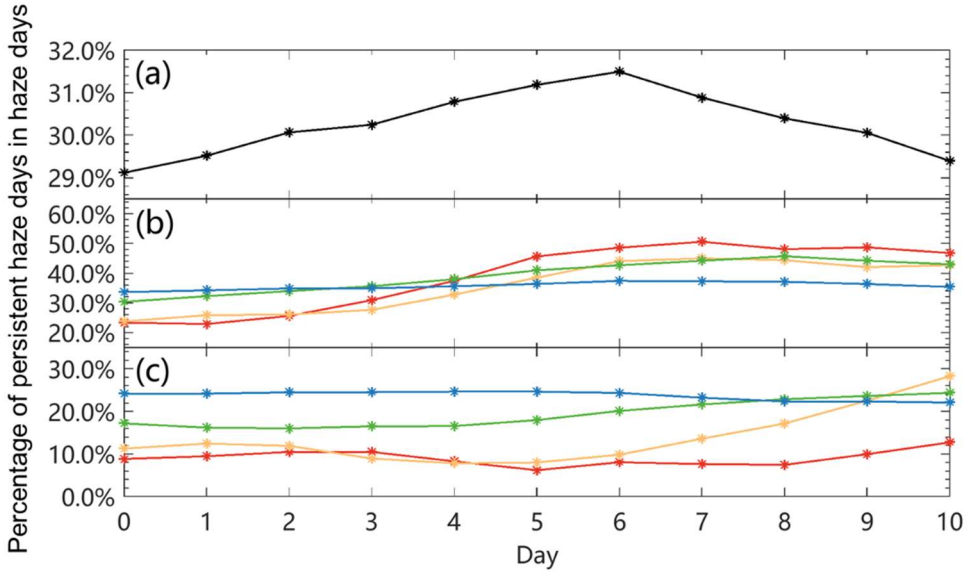

788

789 **Figure 7.** The percentage of persistent haze days in haze days at Day *i* (*i* = 0…10) on the condition
790 that **(a)** the state of the WNAO is unknown, **(b)** the five-day moving average WNAO index is above
791 the 95th (red), 90th (yellow), 75th (green) and 50th (blue) percentiles of the moving average series,
792 and **(c)** when the five-day moving average WNAO index is below the 50th (blue), 25th (green), 10th
793 (yellow) and 5th (red) percentiles of the moving average series.

794

795

796

797

798

799

800

801

802

803

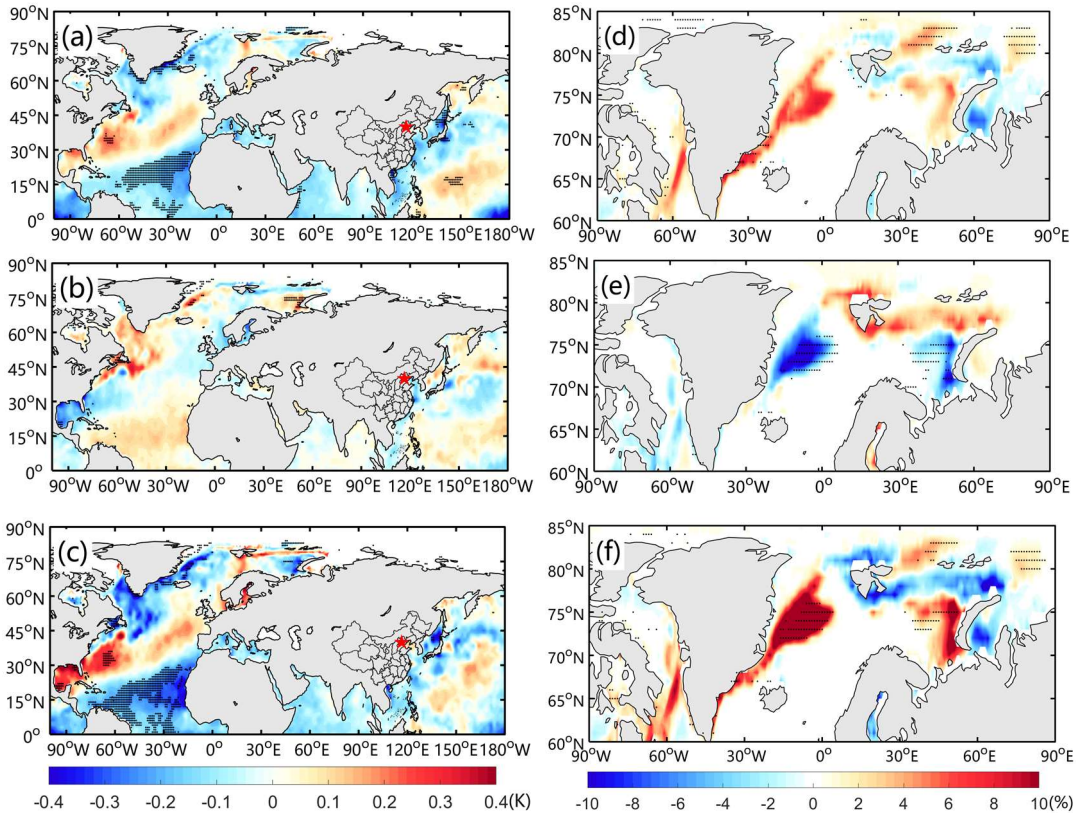

Figure 8. Composite SST anomalies and SIC anomalies for **(a, d)** winters (1988, 1996, 1998, 2005, 2007, 2008, 2011–2015) with the greatest number of persistent haze days and **(b, e)** winters (1980, 1982–1984, 1986, 1987, 1994, 1995, 1999, 2003, 2010) with the lowest number of persistent haze days, and **(c, f)** their differences. The dotted areas show values that are above the 95% confidence level based on a Monte Carlo test with 10,000 simulations.

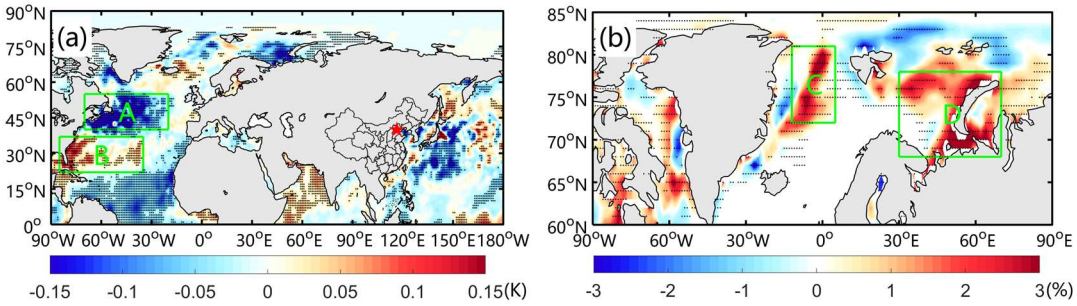

Figure 9. (a) Composite SST anomalies and **(b)** SIC anomalies for the 10 days before the first day of the 65 persistent haze events. The dotted areas show values that are above the 95% confidence level based on a two-sided Student's *t*-test. The green rectangles A and B in **(a)** denote a north region (40° N–55° N, 70° W–20° W) and a south region (22° N–37° N, 85° W–35° W) over the North Atlantic, and the green rectangles C and D in **(b)** denote the Greenland Sea (12° W–5° E, 72° N–81° N) and the Barents–Kara Sea (30° E–70° E, 68° N–78° N), respectively.

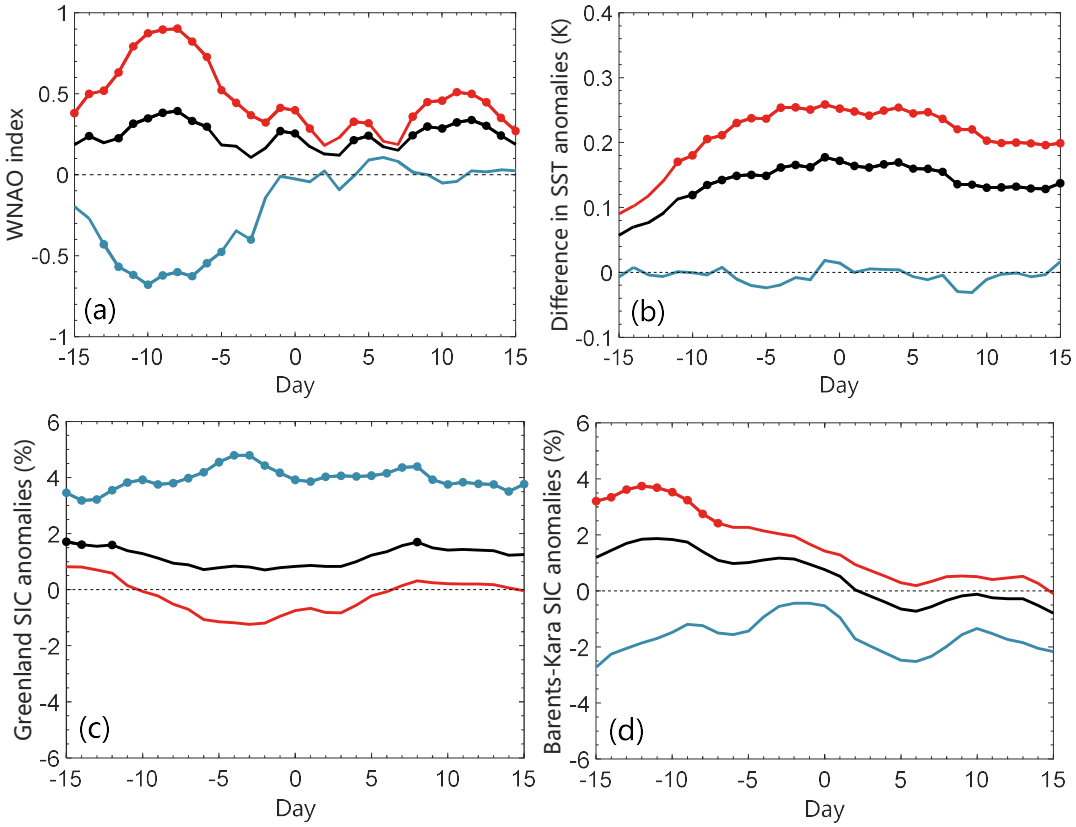

Figure 10. Composite daily time series of the **(a)** WNAO index, **(b)** difference in the SST anomalies over the two regions, as presented in Figure 9a, **(c, d)** region-averaged SIC anomalies in the **(c)** Greenland Sea (marked by C in Figure 9b) and **(d)** Barents–Kara Sea (marked by D in Figure 9b) for the 65 persistent haze events (black), 43 WNAO+-related persistent haze events (red) and 22 WNAO−-related persistent haze events (blue) from Day −15 to Day 10. The difference in the SST anomalies is calculated by subtracting the region-averaged SST anomalies in the north (rectangle A) from the region-averaged SST anomalies in the south (rectangle B) (that is, B minus A). A persistent haze event that is related to the WNAO+ (WNAO−) is selected when its averaged WNAO index is positive (negative) from Day -10 to Day -6 of the persistent haze event.